



^1H , ^{13}C and ^{15}N resonance assignment of the YTH domain of YTHDC2

Fahu He^{1,2} · Ryuta Endo^{1,2} · Kanako Kuwasako^{1,2,3} · Mari Takahashi^{1,2} · Kengo Tsuda^{1,2} · Takashi Nagata^{1,4,5} · Satoru Watanabe^{1,6} · Akiko Tanaka^{1,2} · Naohiro Kobayashi^{1,7} · Takanori Kigawa^{1,6} · Peter Güntert^{8,9,10} · Mikako Shirouzu^{1,2} · Shigeyuki Yokoyama^{1,11} · Yutaka Muto^{1,2,3}

Received: 11 July 2020 / Accepted: 5 September 2020 / Published online: 15 September 2020
© Springer Nature B.V. 2020

Abstract

In humans, YTH (YT521-B homology) domain containing protein 2 (YTHDC2) plays a crucial role in the phase-shift from mitosis to meiosis. YTH domains bind to methylated adenosine nucleotides such as m^6A . In a phylogenetic tree, the YTH domain of YTHDC2 (YTH2) and that of the YTH containing protein YTHDC1 (YTH1) belong to the same sub-group. However, the binding affinity of m^6A differs between these proteins. Here, we report ^1H , ^{13}C and ^{15}N resonance assignment of YTH2 and its solution structure to examine the difference of the structural architecture and the dynamic properties of YTH1 and YTH2. YTH2 adopts a $\beta 1-\alpha 1-\beta 2-\alpha 2-\beta 3-\beta 4-\beta 5-\alpha 3-\beta 6-\alpha 4$ topology, which was also observed in YTH1. However, the $\beta 4-\beta 5$ loops of YTH1 and YTH2 are distinct in length and amino acid composition. Our data revealed that, unlike in YTH1, the structure of m^6A -binding pocket of YTH2 formed by the $\beta 4-\beta 5$ loop is stabilized by electrostatic interaction. This assignment and the structural information for YTH2 will provide the insight on the further functional research of YTHDC2.

Keywords YTH domain · YTHDC2 · RNA binding domain · Spermatogonium · N^6 -methylated adenosine · Meiosis

The chemical shift assignments for the YTH domain of YTHDC2 have been deposited in the BMRB database with the accession no. 36310. The atomic coordinates for the ensemble of 20 NMR structures of YTH2 calculated by CYANA 2.1 have been deposited in the Protein Data Bank (accession code 2YU6) and those with Amber12 refinement in the Protein Data Bank (accession code 6LR2).

Fahu He and Ryuta Endo have contributed equally to this work.

Electronic supplementary material The online version of this article (doi:<https://doi.org/10.1007/s12104-020-09974-3>) contains supplementary material, which is available to authorized users.

✉ Shigeyuki Yokoyama
yokoyama@riken.jp

✉ Yutaka Muto
ymuto@musashino-u.ac.jp

¹ RIKEN Center for Life Science and Technologies, 1-7-22 Suehiro-cho, Tsurumi-ku, Yokohama 230-0045, Japan

² RIKEN, Systems and Structural Biology Center, 1-7-22 Suehiro-cho, Tsurumi, Yokohama 230-0045, Japan

³ Faculty of Pharmacy and Research Institute of Pharmaceutical Sciences, Musashino University, Tokyo 202-8585, Japan

Biological context

In human cells, YTH (YT521-B homology) domain containing protein 2 (YTHDC2) binds to the mRNAs rich with N^6 -methyladenosines (m^6A) along with the meiosis-specific coiled-coil domain-containing protein (MEIOC). Simultaneously, YTHDC2 recruits the 5′–3′ exonuclease 1 (XRN1) and interact with the small ribosomal subunit to accelerate the degradation of the modified mitotic mRNAs (Wojtas et al. 2017; Jain et al. 2018; Kretschmer et al. 2018). YTHDC2 is also reportedly involved in stabilization of the

⁴ Institute of Advanced Energy, Kyoto University, Gokasho, Uji, Kyoto 611-0011, Japan

⁵ Graduate School of Energy Science, Kyoto University, Gokasho, Uji, Kyoto 611-0011, Japan

⁶ Present Address: RIKEN Quantitative Biology Center, 1-7-22 Suehiro-cho, Tsurumi-ku, Yokohama 230-0045, Japan

⁷ Present Address: RIKEN SPring-8 Center, Yokohama 230-0045, Japan

⁸ Tatsuo Miyazawa Memorial Program, RIKEN Genomic Sciences Center, Yokohama 230-0045, Japan

meiosis-specific mRNAs for later use with other factors such as Y-box binding protein 2 MSY2 and PIWI family protein MIWI (Bailey et al. 2017). Through these interactions, YTHDC2 plays a crucial role in the phase-shift from mitosis to meiosis.

YTHDC2 has a so-called YTH domain at its C-terminus, which is annotated as containing ~130 amino acid residues in the Pfam (PF07177) (<http://pfam.xfam.org/>), Prosite (PS50882) (<https://prosite.expasy.org/>) and InterPro (IPR007275) databases (Mulder et al. 2007). It has been determined that YTH domain is the specific protein module that recognizes m⁶A in RNA molecules for the control of the RNA metabolism (Liao et al. 2018). In addition, some YTH domains could also bind to N¹-methyladenosine (m¹A) (Dai et al. 2018).

In human, five YTH containing proteins, YTHDF1–3 (YTH domain-containing family proteins 1–3) and YTHDC1–2 (YTH domain containing protein 1–2) have been identified (Supplementary Fig. 1). In a phylogenetic tree, the YTH domains of YTHDC1 and YTHDC2 (hereafter termed YTH1 and YTH2 respectively) were in the same subgroup and those of YTHDF1–3 belonged to another group (Liao S et al. 2018). The primary structure conservation is quite high among YTH domains of YTHDF1–3, and all of them exhibit similar binding to both m⁶A and m¹A (Dai et al. 2018; Li et al. 2014; Zhu et al. 2014). However, comparing the amino acid sequences of YTH1 and YTH2, the region spanning residues S419–M438 in YTH1, which is necessary for the formation of the m⁶A binding pocket, is quite different from the corresponding region (I1352–G1264) of YTH2 (Supplementary Fig. 1). Moreover, YTH1 exhibits strong affinity for m⁶A and it can also bind to m¹A, but the binding affinity of YTH2 for m⁶A is not as strong and YTH2 can not bind to m¹A (Liao et al. 2018; Dai et al. 2018).

Recently, crystal structure of the YTH domain of YTHDC2 has been reported (Ma et al. 2019). Thus, additional solution structural information by NMR method could be the basis for further functional analysis for YTHDC2. Here we report the ¹H, ¹³C and ¹⁵N assignment and the structure of YTH2 and also compared the dynamic properties of YTH1 and YTH2 based on ¹H–¹⁵N relaxation data to elucidate the architecture of the m⁶A-binding pocket of YTH2.

This assignment and the structural information for YTH2 will provide the insight on the further understanding of the YTHDC2 function.

Methods and experiments

Sample preparation

In our work, a cDNA clone with a natural variation (an L1409Q mutation), which was deposited as rs1132528 in the dbSNP database (<https://www.ncbi.nlm.nih.gov/snp/rs1132528>) (Ota et al. 2004), was used for plasmid construction. We produced a soluble YTH2 domain spanning residues 1288–1421 (Supplementary Fig. 1). The folding state of the protein was checked by 2D ¹H–¹⁵N HSQC experiments with ¹⁵N-labeled samples (Kigawa et al. 2004). We also prepared the YTH domain of YTHDC1 (YTH1) spanning residues 355–495 for ¹H–¹⁵N relaxation experiments.

¹⁵N/¹³C-labeled YTH1 and YTH2 were synthesized using an *Escherichia coli* cell-free protein synthesis system (Kigawa et al. 2004; Matsuda et al. 2007) and were treated and purified as described previously (Li et al. 2008). The samples were expressed as N-terminally His-tag fusion proteins. The fusion proteins were purified by Ni-NTA affinity column. The His-tag was released by TEV protease cleavage and the YTH domain fragments were further purified by Superdex 75 gel filtration chromatography (GE Healthcare). For structure determination, uniformly ¹⁵N/¹³C-labeled YTH samples were concentrated to nearly 1.0 mM in 20 mM Tris-HCl (Tris-d₆) buffer (pH 7.0), containing 100 mM NaCl, 1 mM dithiothreitol, and 0.02% Na₃N with the addition of ²H₂O to 10% v/v.

NMR spectroscopy and structure calculations

All NMR data were acquired at 293 and 298 K on Bruker 700 MHz and Bruker 800 MHz spectrometers. All NMR data were processed with *NMRPipe* software (Delaglio et al. 1995). Two-dimensional ¹H–¹³C and ¹H–¹⁵N HSQC spectra, three-dimensional HNC(O), HN(CA)CO, HNCA, HN(CO)CA, HNCACB, CBCA(CO)NH, HBHA(CO)NH, H(CCCO)NH, (H)CC(CO)NH, HCCH-TOCSY, HCCH-COSY, CCH-TOCSY and NOESY spectra (Clare and Gronenborn 1998) were used to assign all carbon, nitrogen and hydrogen atoms of the proteins.

NOE peaks from ¹⁵N and ¹³C-edited 3D NOESY spectra with 80 ms mixing time were converted to distance restraints for structure calculations for YTH2. The three-dimensional structures of the protein were determined by combined automated NOESY cross peak assignment and structure

⁹ Institute of Biophysical Chemistry and Frankfurt Institute of Advanced Studies, Goethe-University Frankfurt, Max-von-Laue-Str.9, 60438 Frankfurt am Main, Germany

¹⁰ Graduate School of Science and Technology, Tokyo Metropolitan University, 1-1 Minami-Ohsawa, Hachioji, Tokyo 192-0397, Japan

¹¹ RIKEN Structural Biology Laboratory, 1-7-22 Suehiro-cho, Tsurumi-ku, Yokohama 230-0045, Japan

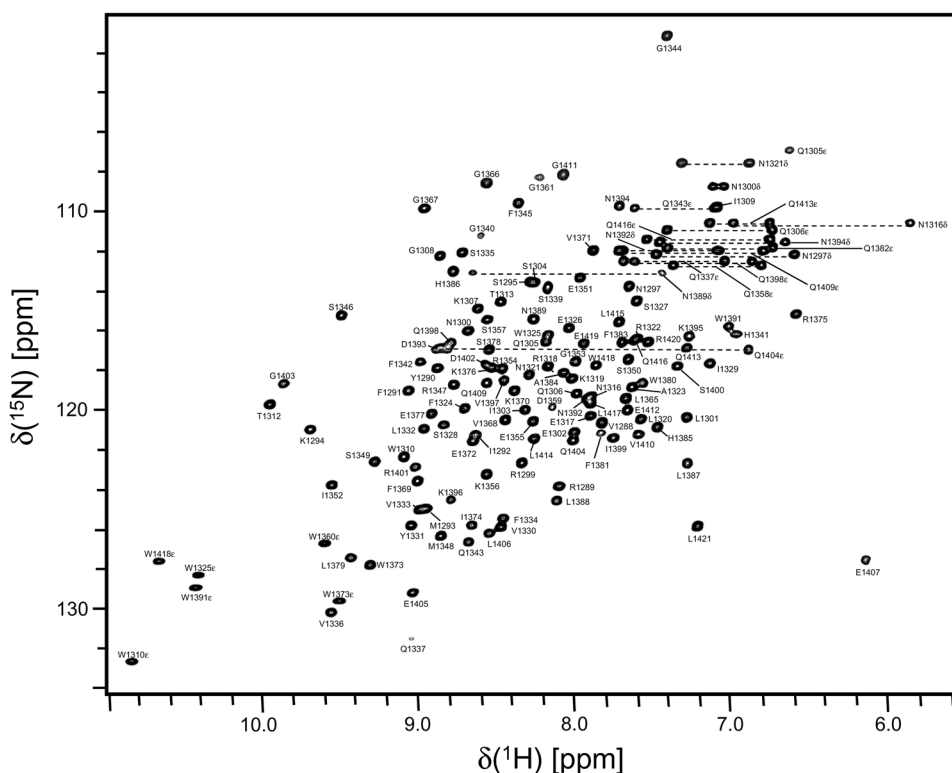
calculation with torsion angle dynamics (Herrmann et al. 2002) implemented in the program CYANA 2.1 (Güntert et al. 1997). Dihedral angle constraints for φ and ψ were obtained from the main-chain and $^{13}\text{C}^\beta$ chemical shift values using the program TALOS (Cornilescu et al. 1999) and by analyzing the NOESY spectra. Stereospecific assignments for isopropyl methyl and methylene groups were determined based on the patterns of the inter- and intra-residual NOE intensities. The structure calculations started from 200 randomized conformers and used the standard CYANA simulated annealing schedule, with 40,000 torsion angle dynamics steps per conformer. Among them, the 20 structures with the lowest CYANA target function values were deposited in the Protein Data Bank (accession code 2YU6).

Further refinements by restrained molecular dynamics followed by restrained energy minimization were performed for the 40 conformers with the lowest final CYANA target function values, using the Amber12 program with the Amber 2012 force field and a generalized Born model (Case et al. 2005), as described previously. The 20 conformers with the lowest Amber energy values were selected. They were deposited in the Protein Data Bank (accession code 6LR2). For the 20 final structures, PROCHECK-NMR (Laskowski et al. 1996) and MOLMOL (Koradi et al. 1996) were used to validate and to visualize the final structures, respectively.

Measurements for ^1H - ^{15}N dynamics parameters

In order to perform the dynamics experiment for YTH1, the ^1H - ^{15}N assignment of YTH1 was referred to the BMRB data base with accession no. 25188 (Theler et al. 2014). For both of YTH1 and YTH2, measurements of nitrogen relaxation times, T_1 and T_2 , and proton–nitrogen heteronuclear NOEs were performed on a 600 MHz spectrometer with a cryo-probe (Bruker AV 600) at 25 °C. Eight different relaxation delays were recorded for the ^{15}N T_1 (T_1 delays = 5, 65, 145, 246, 366, 527, 757, and 1148 ms) and ^{15}N T_2 (T_2 delays = 32, 48, 64, 80, 96, 112, 128, and 144 ms) relaxation experiments. The ^{15}N T_1 and ^{15}N T_2 values were extracted using a curve-fitting subroutine included in the Sparky program (T. D. Goddard and D. G. Kneller, SPARKY 3, University of California, San Francisco). For the steady-state ^1H - ^{15}N NOE measurement, a relaxation delay of 3 s and a ^1H presaturation time of 3 s were used in the NOE experiment, and a 6 s relaxation delay was used in the reference experiment. NMR peak heights determined by Sparky were used for the program ‘sparky2rate’ (<http://ursula.chem.yale.edu/~lorialab/software.php>). The proton–nitrogen heteronuclear NOE values were calculated as the ratio between the cross-peak intensities with (I) and without (I_0) ^1H

Fig. 1 ^1H - ^{15}N HSQC spectra of YTHDC2 on Bruker 800 MHz spectrometer. Each signal is labeled with the assignment



saturation (III_0). The errors were estimated from the root mean square of the baseline noise in the two spectra (Farrow et al. 1994).

Extent of assignment and data deposition

Resonance assignments and NMR structure determination

The assigned ^1H - ^{15}N HSQC spectrum of YTH2 has been depicted in Fig. 1. For YTH2, the backbone and side chain resonance assignments are almost complete, except for the amide protons of Ser1296, Leu1298, Ser1311, Ser1315, Gly1338, Gln1358, Ser1362, Ala1363, Gly1364, and Gln1382, C^δ , C^ϵ , and C^ζ of Phe1345, $\text{H}\beta$ of Arg1318 and $\text{H}\alpha$ of Gly1338. All side chain NH_2 resonances of Asn/Gln residues were assigned and all X-Pro peptide bonds were confirmed to be in the *trans* conformation.

The quality of the NOESY spectrum of YTH2 is appropriate for the straight-forward structural calculation. In the ^{15}N - and ^{13}C -edited 3D NOESY, 3171 non-redundant distance restraints, including 1252 long-range distance restraints were identified, and the backbone torsion angle restraints calculated by the TALOS program (Cornilescu et al. 1999) were also used for structure calculations with the program CYANA 2.1 (Herrmann et al. 2002; Güntert et al. 1997; Güntert 2004) and Amber12 (Case et al. 2005).

The precision of the bundle of 20 conformers that represent the solution structure of the YTH2 domain is characterized by RMSD values to the mean coordinates for residues 1288–1295, 1341–1352, 1360–1392, and 1395–1421 (corresponding to the secondary elements and excluding the seven amino acid tag-region at the N-terminus) of 0.35 Å for the backbone atoms and 0.96 Å for all heavy atoms (Supplementary Fig. 1 and Fig. 2a and b). The structural quality is also reflected by the fact that 90.6% of the (φ, ψ) backbone torsion angle pairs are in the most favored and additionally allowed regions of the Ramachandran plot, according to the program PROCHECK-NMR (Laskowski et al. 1996). Statistics regarding the quality and precision of the final 20 best conformers that represent the solution structures of the YTH2 domain are given in Supplementary Table 1.

Solution structures of the YTH domain of YTHDC2

The YTH2 domain adopts a $\beta 1$ - $\alpha 1$ - $\beta 2$ - $\alpha 2$ - $\beta 3$ - $\beta 4$ - $\beta 5$ - $\alpha 3$ - $\beta 6$ - $\alpha 4$ topology ($\beta 1$:R1289–S1295, $\alpha 1$:R1299–K1307, $\beta 2$:G1308–W1310, $\alpha 2$:N1316–E1326, $\beta 3$:V1330–V1336, $\beta 4$:H1341–S1349, $\beta 5$:V1368–L1379, $\alpha 3$:F1381–H1385, $\beta 6$:G1403–L1406, and $\alpha 4$:P1408–L1421) (Supplementary Fig. 1 and Fig. 2a and b). The six β -strands form a cleaved β -barrel structure with order $\beta 6$ - $\beta 1$ - $\beta 3$ - $\beta 4$ - $\beta 5$ - $\beta 2$. The $\alpha 1$ and $\alpha 2$ helices are located at the top and bottom of the β -barrel structure, respectively. The $\alpha 3$ helix and the following region, which contains a small β -hairpin structure ($\beta 5'$ - $\beta 5''$, $\beta 5'$:L1387–N1389, $\beta 5''$: K1395–V1397),

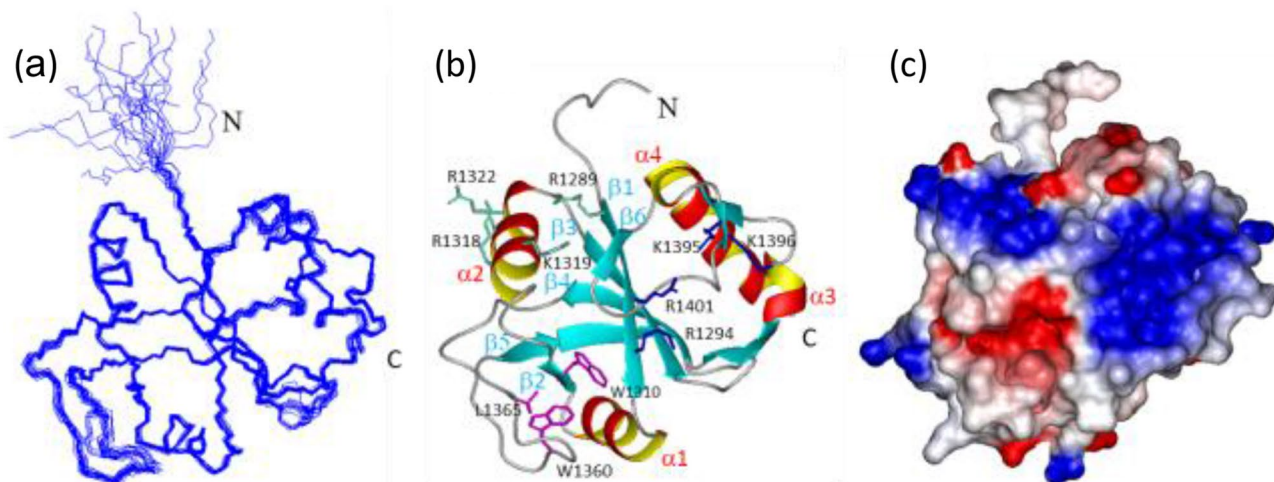


Fig. 2 Solution structure of the YTH domain of YTHDC2. **a** Best-fit superposition of the backbone atoms from the 20 lowest energy structures of YTH2, calculated by CYANA2.1 and Amber12. **b** Ribbon presentation of the lowest energy structure of YTH2. The helices, β -strands, and loop regions are shown in red/yellow, cyan, and gray, respectively. The side-chains of the amino-acid residues that

form the m^6A binding pocket (W1310, W1360 and L1365), the first positively charged patch (R1289, R1318, K1319 and R1322) and the second positively charged patch (R1294, K1395, R1396 and R1401) are colored magenta, sky-blue, and blue, respectively. **c** Electrostatic surface presentation of YTH2. Blue and red represent positive and negative electrostatic surface potentials, respectively

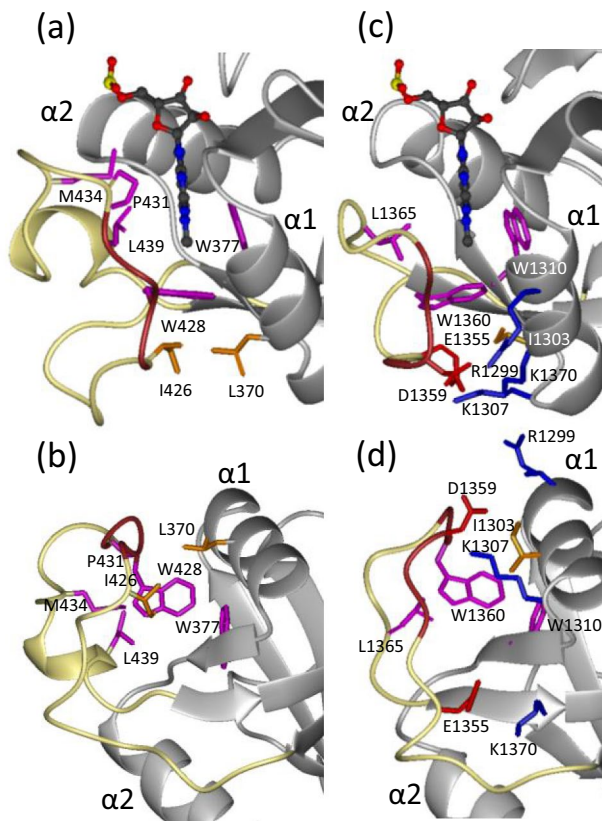


Fig. 3 Comparison of the putative m⁶A binding pockets between YTH1 and YTH2. Expanded presentation of the formation of the m⁶A binding pocket of YTH1 with m⁶A (PDBID:4R3I) (a, b) and of the formation of the putative m⁶A binding pocket of YTH2 (c, d) from two directions. In a, c the m⁶A nucleotide is shown by the ball and stick representation. The m⁶A nucleotide in (c) was deduced based on the m⁶A nucleotide in the structure of YTH1. Within the β 4– β 5 loop main chain (colored light yellow), the segments that exhibit high NOE values are colored brown. The amino acid residues that form the m⁶A-binding pocket, those that sustain the crucial Trp residue in the loop, positively charged amino acid residues, and acidic residues are colored magenta, dark orange, blue and red, respectively

associates with helix α 4 and partially covers the side surface of the β -barrel structure corresponding to the area on strands β 6– β 1– β 3– β 4 (Fig. 2a and b). These structural features are common with the previously-solved structures of the YTH domains of YTHDC1 and YTHDF2 (Li et al. 2014; Zhu et al. 2014; Theler et al. 2014; Xu et al. 2015).

In the YTH2 domain, two positively charged patches are formed on the surface. One is formed by residues R1289 (β 1), R1318 (α 2), K1319 (α 2) and K1322 (α 2) (Supplementary Fig. 1 and Fig. 2b and c). The second is formed by residues K1294 (β 1), K1395, K1396, and R1401 (just before β 6) (Supplementary Fig. 1 and Fig. 2b and c). Notably, the positively charged amino acid residues in the second patch (K1294 and R1401) are well-conserved among the YTH domains that use the modified nucleotide recognition pocket described below. However, the YTH domain of yeast

YTH-containing protein, Mmi1 (Wang et al. 2016), which recognizes the target RNA without the pocket, lacks both of these positively charged residues. Thus, these two amino acid residues are considered to be important for the use of the deep pocket structure for RNA recognition.

Among the five YTH domains derived from YTHDC1–2 and YTHDF1–3, the long loops between the strands β 4 and β 5 (the β 4– β 5 loop) are considered to be involved in the formation of the m⁶A (and m¹A) binding pocket along with amino acids located on the α 2 helix and the β 2 strand (Li et al. 2014; Zhu et al. 2014; Theler et al. 2014; Xu et al. 2015). Reportedly, in YTH1, W377 (β 2), W428 (β 4– β 5 loop) and L439 (β 4– β 5 loop) constitute the characteristic pocket structure (Fig. 3a and b) (Theler et al. 2014; Xu et al. 2015). The spatial positions corresponding to W377, W428 and L439 in YTH1 were occupied in YTH2 by W1310 in β 2 and W1360 and L1365 in the β 4– β 5 loop, respectively to form the m⁶A-binding pocket (Fig. 3c). However, the β 4– β 5 loops of YTH1 and YTH2 are diverse in length and amino acid composition (Supplementary Fig. 1), even though YTH1 and YTH2 belong to the same branch in a phylogenetic tree of YTH domains. To elucidate the architecture of the β 4– β 5 loops, we analyzed the backbone dynamics by measuring backbone ^1H – ^{15}N heteronuclear NOEs and T_1/T_2 values and compared the dynamic properties of the β 4– β 5 loops of YTH1 and YTH2.

Dynamic properties of the YTH1 and YTH2 domains

In the cases for YTH1 and YTH2, ^1H – ^{15}N NOE values of the amino acid residues in α helices and β -strands are \sim 0.80, which are the normal ^1H – ^{15}N NOE values for the amino acid residues in the rigid structural regions. In the case of YTH1, within the β 4– β 5 loop (S417–G442) (Supplementary Fig. 2a), the NOE values are below 0.8. Especially, those for the G423–I426 and A432–M438 segments are \sim 0.60, indicating fast internal motions of these regions. However, the NOE values spanning residues H427–L430, which is sandwiched by the above segments, get nearly back to \sim 0.73, suggesting the fluctuation of the short segment is suppressed. In the case of YTH2, ^1H – ^{15}N resonances originating from the E1355–K1356 gave a lower NOE intensity (\sim 0.60) and the resonances of the S1362–G1364 segments were missing, suggesting a short proton T_2 value caused by chemical exchange. However, the NOE values of S1357, D1359 and G1361 get back to nearly \sim 0.69 (Supplementary Fig. 2b). In both cases, a crucial Trp residues (W428 in YTH1 and W1360 in YTH2) were located in the region with a little bit recovered NOE values, thus it is deduced that the mobility for these Trp residues were suppressed. Supplementary Table II compares the ^1H – ^{15}N heteronuclear NOE values for the NH^e1 of the corresponding Trp residues between YTH1 and

YTH2. Actually, the above-mentioned W428 (YTH1) and W1360 (YTH2) exhibit the similar NOE values (~ 0.7), indicating that they showed a little bit restricted mobility although they are not in the rigid structure. The structural factors that stabilize the segment containing the crucial Trp residues were distinct between the two proteins. Even though YTH1 has a longer $\beta 4$ – $\beta 5$ loop than YTH2, the structure of the H427–L430 segment of YTH1 is fixed more rigidly than the D1359–G1361 segment of YTH2.

In the complex structure of YTH1 with m^6A (Theler et al. 2014; Xu et al. 2015), I426 ($\beta 4$ – $\beta 5$ loop) and L370 ($\alpha 1$) interacted with each other and fixed the aromatic ring of W428, and the side chains of P431 and M434 interacted with L439 and were also involved in the formation of the deep m^6A binding pocket (Fig. 3a). YTH1 is considered to exhibit higher binding affinity for m^6A than YTH2 with many hydrophobic amino acid residues.

In YTH2, the $\beta 4$ – $\beta 5$ loop did not contain such bulky amino acid residues as in YTH1 (Supplementary Fig. 1 and Fig. 3c and d) and the position corresponding to I426 of YTH1 was occupied by D1359. Based on the present YTH2 structure, R1299 and K1307 on the $\alpha 1$ -helix could interact with YTH2-specific D1359 occurring just before the crucial Trp residue (W1360) (Supplementary Fig. 1 and Fig. 3d). In addition, K1370 ($\beta 5$) and YTH2-specific E1355 could form another electrostatic interaction. Thus, in YTH2, the interaction between the $\alpha 1$ helix and the $\beta 4$ – $\beta 5$ loop is mediated by electrostatic interactions, instead of the hydrophobic interaction observed in YTH1. We suggest that the YTH2-specific electrostatic interactions stabilize the loop structure for formation of a shallow m^6A -binding pocket, which could enable fast exchange of the substrate and be suitable for the enzymatic role of YTH2.

Acknowledgements We thank James Allen, DPhil, from Edanz Group (www.edanzediting.com/ac) for editing a draft of this manuscript. We thank Dr. Sumio Sugano in the Department of Medical Genome Sciences, Graduate School of Frontier Sciences, University of Tokyo for providing the cDNA clone with a natural variation YTHDC2 (an L1409Q mutation).

Funding This work was supported by the RIKEN Structural Genomics/Proteomics Initiative (RSGI) and by the National Project on Protein Structural and Functional Analyses of the Ministry of Education, Culture, Sports, Science and Technology of Japan. This work was also supported by grants from Musashino University *Gakuin Tokubetsu Kenkyu* to YM.

Compliance with Ethical Standards

Conflict of interest The authors have no conflict of interest to report.

References

- Bailey AS, Batista PJ, Gold RS, Chen YG, de Rooij DG, Chang HY, Fuller MT (2017) The conserved RNA helicase YTHDC2 regulates the transition from proliferation to differentiation in the germline. *eLife* 6:e26116. <https://doi.org/10.7554/eLife.26116>
- Case DA, Cheatham TE III, Darden T, Gohlke H, Luo R, Merz KM Jr, Onufriev A, Simmerling C, Wang B, Woods RJ (2005) The amber biomolecular simulation programs. *J Comput Chem* 26:1668–1688. <https://doi.org/10.1002/jcc.20290>
- Clore GM, Gronenborn AM (1998) New methods of structure refinement for macromolecular structure determination by NMR. *Proc Natl Acad Sci USA* 95:5891–5898. <https://doi.org/10.1073/pnas.95.11.5891>
- Cornilescu G, Delaglio F, Bax A (1999) Backbone angle restraints from searching a database for chemical shift and sequence homology. *J Biomol NMR* 13:289–302. <https://doi.org/10.1023/a:1008392405740>
- Dai X, Wang T, Gonzalez G, Wang Y (2018) Identification of YTH domain-containing proteins as the readers for N1-methyladenosine in RNA. *Anal Chem* 90:6380–6384. <https://doi.org/10.1021/acs.analchem.8b01703>
- Delaglio F, Grzesiek S, Vuister GW, Zhu G, Pfeifer J, Bax A (1995) NMRPipe: a multidimensional spectral processing system based in UNIX pipes. *J Biomol NMR* 6:277–293. <https://doi.org/10.1007/bf00197809>
- Farrow NA, Muhandiram R, Singer AU, Pascal SM, Kay CM, Gish G, Shoelson SE, Pawson T, Forman-Kay JD, Kay LE (1994) Backbone dynamics of a free and phosphopeptide-complexed Src homology 2 domain studied by ^{15}N NMR relaxation. *Biochemistry* 33:5984–6003. <https://doi.org/10.1021/bi00185a040>
- Güntert P (2004) Automated NMR structure calculation with CYANA. *Methods Mol Biol* 278:353–378. <https://doi.org/10.1385/1-59259-809-9:353>
- Güntert P, Mumenthaler C, Wüthrich K (1997) Torsion angle dynamics for NMR structure calculation with the new program DYANA. *J Mol Biol* 273:283–298. <https://doi.org/10.1006/jmbi.1997.1284>
- Herrmann T, Güntert P, Wüthrich K (2002) Protein NMR structure determination with automated NOE assignment using the new software CANDID and the torsion angle dynamics algorithm DYANA. *J Mol Biol* 319:209–227. [https://doi.org/10.1016/s0022-2836\(02\)00241-3](https://doi.org/10.1016/s0022-2836(02)00241-3)
- Jain D, Puno MR, Meydan C, Lailler N, Mason CE, Lima CD, Anderson KV, Keeney S (2018) Ketu mutant mice uncover an essential meiotic function for the ancient RNA helicase YTHDC2. *eLife* 7:e30919. <https://doi.org/10.7554/eLife.30919>
- Kigawa T, Yabuki T, Matsuda N, Matsuda T, Nakajima R, Tanaka A, Yokoyama S (2004) Preparation of *Escherichia coli* cell extract for highly productive cell-free protein expression. *J Struct Funct Genomics* 5:63–68. <https://doi.org/10.1023/B:JSFG.0000029204.57846.7d>
- Koradi R, Billeter M, Wüthrich K (1996) MOLMOL: a program for display and analysis of macromolecular structures. *J Mol Graph* 14:51–55. [https://doi.org/10.1016/0263-7855\(96\)00009-4](https://doi.org/10.1016/0263-7855(96)00009-4)
- Kretschmer J, Rao H, Hackert P, Sloan KE, Höbartner C, Bohnsack MT (2018) The m^6A reader protein YTHDC2 interacts with the small ribosomal subunit and the 5'–3' exoribonuclease XRN1. *RNA* 24:1339–1350. <https://doi.org/10.1261/rna.064238.117>
- Laskowski RA, Rullmann JA, MacArthur MW, Kaptein R, Thornton JM (1996) AQUA and PROCHECK-NMR: programs for checking the quality of protein structures solved by NMR. *J Biomol NMR* 8:477–486. <https://doi.org/10.1007/bf00228148>
- Li H, Koshiba S, Hayashi F, Tochio N, Tomizawa T, Kasai T, Yabuki T, Motoda Y, Harada T, Watanabe S, Inoue M, Hayashizaki Y, Tanaka A, Kigawa T, Yokoyama S (2008) Structure of the C-terminal

- phosphotyrosine interaction domain of Fe65L1 complexed with the cytoplasmic tail of amyloid precursor protein reveals a novel peptide binding mode. *J Biol Chem* 283:27165–27178. <https://doi.org/10.1074/jbc.M803892200>
- Li F, Zhao D, Wu J, Shi Y (2014) Structure of the YTH domain of human YTHDF2 in complex with an m(6)A mononucleotide reveals an aromatic cage for m(6)A recognition. *Cell Res* 24:1490–1492. <https://doi.org/10.1038/cr.2014.153>
- Liao S, Sun H, Xu C (2018) YTH Domain: A Family of N6-methyladenosine (m6A) Readers. *Genomics Proteom Bioinform* 16:99–107. <https://doi.org/10.1016/j.gpb.2018.04.002>
- Ma C, Liao S, Zhu Z (2019) Crystal structure of human YTHDC2 YTH domain. *Biochem Biophys Res Commun* 518:678–684. <https://doi.org/10.1016/j.bbrc.2019.08.107>
- Matsuda T, Koshiha S, Tochio N, Seki E, Iwasaki N, Yabuki T, Inoue M, Yokoyama S, Kigawa T (2007) Improving cell-free protein synthesis for stable-isotope labeling. *J Biomol NMR* 37:225–229. <https://doi.org/10.1007/s10858-006-9127-5>
- Mulder NJ, Apweiler R, Attwood TK, Bairoch A, Bateman A, Binns D, Bork P, Buillard V, Cerutti L, Copley R, Courcelle E, Das U, Daugherty L, Dibley M, Finn R, Fleischmann W, Gough J, Haft D, Hulo N, Hunter S, Kahn D, Kanapin A, Kejariwal A, Labarga A, Langendijk-Genevaux PS, Lonsdale D, Lopez R, Letunic I, Madera M, Maslen J, McAnulla C, McDowall J, Mistry J, Mitchell A, Nikolskaya AN, Orchard S, Orengo C, Petryszak R, Selengut JD, Sigrist CJA, Thomas PD, Valentin F, Wilson D, Wu CH, Yeats C (2007) New developments in the InterPro database. *Nucleic Acids Res* 35(Database issue):D224–D228. <https://doi.org/10.1093/nar/gkl841>
- Ota T, Suzuki Y, Nishikawa T, Otsuki T, Sugiyama T, Irie R, Wakamatsu A, Hayashi K, Sato H, Nagai K, Kimura K, Makita H, Sekine M, Obayashi M, Nishi T, Shibahara T, Tanaka T, Ishii S, Sugano S (2004) Complete sequencing and characterization of 21,243 full-length human cDNAs. *Nat Genet* 36:40–45. <https://doi.org/10.1038/ng1285>
- Theler D, Dominguez C, Blatter M, Boudet J, Allain FH (2014) Solution structure of the YTH domain in complex with N6-methyladenosine RNA: a reader of methylated RNA. *Nucleic Acids Res* 42:13911–13919. <https://doi.org/10.1093/nar/gku1116>
- Wang C, Zhu Y, Bao H, Jiang Y, Xu C, Wu J, Shi Y (2016) A novel RNA-binding mode of the YTH domain reveals the mechanism for recognition of determinant of selective removal by Mmi1. *Nucleic Acids Res* 44:969–982. <https://doi.org/10.1093/nar/gkv1382>
- Wojtas MN, Pandey RR, Mendel M, Homolka D, Sachidanandam R, Pillai RS (2017) Regulation of m⁶A Transcripts by the 3'/5' RNA Helicase YTHDC2 is essential for a successful meiotic program in the mammalian germline. *Mol Cell* 68:374–387. <https://doi.org/10.1016/j.molcel.2017.09.021>
- Xu C, Wang X, Liu K, Roundtree IA, Tempel W, Li Y, Lu Z, He C, Min J (2015) Structural basis for selective binding of m⁶A RNA by the YTHDC1 YTH domain. *Nat Chem Biol* 10:927–929. <https://doi.org/10.1038/nchembio.1654>
- Zhu T, Roundtree IA, Wang P, Wang X, Wang L, Sun C, Tian Y, Li J, He C, Xu Y (2014) Crystal structure of the YTH domain of YTHDF2 reveals mechanism for recognition of N6-methyladenosine. *Cell Res* 24:1493–1496. <https://doi.org/10.1038/cr.2014.152>

Publisher's Note Springer Nature remains neutral with regard to jurisdictional claims in published maps and institutional affiliations.